
**Separation Science and Technology**
Publication details, including instructions for authors and subscription information:
http://www.informaworld.com/smpp/title~content=t713708471

# Characteristics of $NO_x$ adsorption and surface chemistry on impregnated activated carbon

Young-Whan Lee[a]; Dae-Ki Choi[a]; Jin-Won Park[b]
[a] Environment and Process Technology Division, Korea Institute of Science and Technology, Seoul, South Korea [b] Department of Chemical Engineering, Yonsei University, Seoul, South Korea

Online publication date: 23 April 2002

SEPARATION SCIENCE AND TECHNOLOGY, 37(4), 937–956 (2002)

# CHARACTERISTICS OF $NO_x$ ADSORPTION AND SURFACE CHEMISTRY ON IMPREGNATED ACTIVATED CARBON

**Young-Whan Lee,[1,*] Dae-Ki Choi,[1] and Jin-Won Park[2]**

[1]Environment and Process Technology Division,
Korea Institute of Science and Technology, P.O. Box 131,
Cheongryang, Seoul 130-650, South Korea
[2]Department of Chemical Engineering, Yonsei University,
Seoul 120-749, South Korea



## ABSTRACT

Adsorption characteristics of $NO_x$ were studied with granular activated carbon (GAC) impregnated with potassium hydroxide (KOH). To confirm the selective adsorptivity of KOH-impregnated activated carbon (K-IAC) to $NO_x$ in a fixed-bed adsorption column, temperature of 303–403K, linear velocity of 10–32 cm/sec, and effect of added oxygen were observed. Using scanning electron microscopy (SEM), time of flight secondary ion mass spectrometry (ToF-SIMS), and SIMS depth profile, surface-reaction phenomena of adsorbent, caused by the KOH impregnation and $NO_x$ adsorption, were investigated. $NO_2$ adsorbs by chemical reaction with impregnated KOH, from which NO is generated. When oxygen exists, the NO again adsorbs to $NO_2$ with oxygen chemisorbed on the surface, which increases the adsorptivity. In the results of ToF-SIMS and SIMS depth profile,

*Corresponding author. Fax: (822) 958-5879; E-mail: ywleek@kistmail.kist.re.kr

$NO_2^-$ and $NO_3^-$ increased at the surface distribution by forming oxide crystals of $KNO_2$ and $KNO_3$ due to bond formation with potassium ions. The SIMS depth profile of $KO^-$ ensured that KOH provided the selective adsorption site of $NO_x$. In the mechanism studied, the basic character was led on K-IAC by surface basic $OH^-$ ions of KOH, oxidation rate from $KNO_2$ to $KNO_3$ was delayed, and adsorptivity of K-IAC to $NO_x$ was improved.

*Key Words*: $NO_x$; KOH; Impregnated activated carbon; Time of flight secondary ion mass spectrometry; Adsorption; Surface chemistry



## INTRODUCTION

The source of $NO_x$ can be classified broadly into both stationary and mobile sources. In this study, combustion flue gas was selected as the object of stationary source. Main $NO_x$ control techniques that are utilized commercially are selective catalytic reduction (SCR) and selective noncatalytic reduction (SNCR). However, these methods have a few problems. First, the SCR has a problem of catalytic deactivation caused by the catalyst poisoning and requires high installation and maintenance fees. On the other hand, SNCR requires a range of operation temperatures that is higher and narrower than that of SCR. Secondly, these methods cannot be applied to $NO_x$ such as the fuel gas, which has a low concentration level (1–3).

In general, the adsorption method not only requires small electrical consumption but also does not generate secondary pollution. In addition, it has merits in that its design is simple and requires only a small space when installed. Granular activated carbon (GAC) has been used widely in treating harmful gas in the air due to its hydrophobic property, high surface area, and intrinsic pore structure. Granular activated carbon has high adsorption capacity towards volatile organic compounds that have low concentrations. But it is observed that it has relatively low adsorptivity toward some inorganic compounds such as $NO_x$ (4–15). Due to this, studies are being conducted for the last several years on impregnated activated carbon to which chemical activity is given by a method that impregnates selective chemical substances.

In terms of the choice of impregnant, those that form stable chemical compounds or modify into harmless gas through a chemical reaction with $NO_x$ should be selected. Studies conducted so far report that adding of basic functional group has a good efficiency level on the selective adsorption of $NO_x$ (16–20). Alkali and alkali-metal compounds have been utilized for catalysis for a long time. Theoretical substance of this catalysis is known as basic surface $OH^-$ ions



MARCEL DEKKER, INC.
270 Madison Avenue, New York, New York 10016

caused by alkaline metal hydroxides (21). In this study, KOH is selected because it is known as the most basic alkaline metal hydroxide among all hydroxides.

Time of flight secondary ion mass spectrometry (ToF-SIMS) is an attractive choice for studies of surface chemistry because it offers extreme surface sensitivity, very low detection limits (ppm or ppb), and, when combined with the time-of-flight capability, permits very high mass resolution to differentiate similar mass fragments. Despite these obvious advantages, there has been little work published on the use of ToF-SIMS in adsorption studies (22). Thus, the surface chemistry on KOH-impregnated activated carbon (K-IAC) before and after $NO_x$ adsorption was examined by performing ToF-SIMS and SIMS depth profile.

The purpose of this study was, through a breakthrough experiment by use of fixed-bed adsorption column, to examine selective adsorption characteristics and surface chemistry according to $NO_x$ that was adsorbed on K-IAC.



## EXPERIMENTAL

### Preparation of KOH Impregnated Activated Carbons

The adsorbent was prepared by impregnating KOH (Junsei Chemical Co., Japan) solution into GAC obtained from coconut shell (Dongyang Carbon Co., Korea). The GAC was sieved through a 8/16 mesh and treated with $N_2$ flowing for an hour at 383K, and then for 4 hr at 413K. Next, the treated GAC was dried at 383K. KOH was impregnated in an aqueous solution state into the GAC via incipient wet impregnation (by mixing 15 g of GAC with a 10 *M* KOH solution in a 500-mL glass-stoppered flask). The flask was immersed in a constant-temperature shaker bath, with a shaker speed of 100 rpm. The mixing was performed at 85°C and lasted for 3 hr. After mixing, the GAC slurry was subjected to vacuum drying at 383K. Thereafter, the sample was filtered, washed with distilled water, and dried at 403K. The KOH-impregnated sample was activated in a stainless-steel column placed in a vertical furnace under a stream of purified $N_2$, with a flow rate of 100 mL/min. Manufactured K-IAC was stored in a desiccator to prevent adsorbent function reduction by common airborne moisture and contaminants. At this time, precautions were taken for impregnation, drying, and storage of adsorbent because the processes have great influence on the adsorption capacity. In order to analyze quantitatively the amount of impregnated potassium on K-IAC, impregnated activated carbon was crushed to less than 100 $\mu$m. Then, a mixture of 0.1 g of the sample and 5 mL of nitric acid was heated for 30 min at 353K. Then it was boiled at 423K until it turned into a gel. After elution of the sample was finished, 50 mL of distilled water was added for filtering. Then, the amount of impregnated potassium was analyzed via atomic



MARCEL DEKKER, INC.
270 Madison Avenue, New York, New York 10016

absorption spectrophotometry (AAS). Through AAS analysis, potassium loading of K-IAC was confirmed to be 9.96 wt%.

## Apparatus and Method

The fixed-bed adsorption system used in this experiment is shown in Fig. 1. Material of the fixed-bed adsorption column was a 316 stainless-steel tube, with an inside diameter of 10.9 mm, and 400 mm length. Inside the columns, a steel mesh was placed in the upper and lower extremities of the adsorbent to support the samples and minimize channeling phenomenon. Temperature of the column was maintained with an electric furnace located at its outer wall. For the system line, temperature was maintained by using a heat band and heat insulating material and was regulated with a proportional-integral-differential (PID) temperature controller (Hanyoung Electronic Co., HY-100, Korea). The temperature was measured by connecting a K-type thermocouple (Omega Engineering Inc.), located inside the line, to a recorder. Each certified 2% $NO/N_2$ and 5000 ppm $NO_2/N_2$ was diluted to the desired concentration range of near 150 and 262 ppm via a mass flow controller (Brooks Co., 5280E, Japan). Purified air containing 20.9% $O_2$ was used for the experiment via the addition of oxygen. In the fore end of the adsorption column, an in-line static mixer was installed to

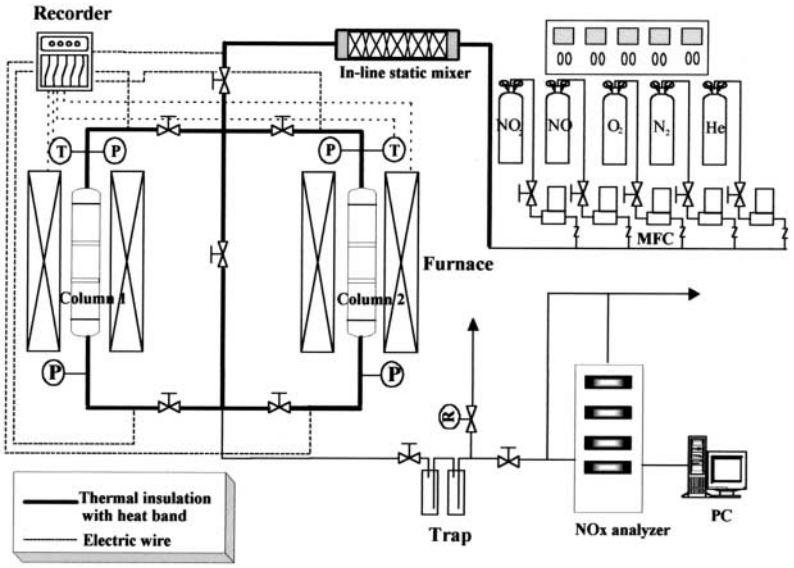


***Figure 1.*** Schematic diagram of the experimental system.





MARCEL DEKKER, INC.
270 Madison Avenue, New York, New York 10016

facilitate mixing. Concentrations of NO and $NO_2$, which exhausted from the bypass line and adsorption column, were analyzed by using a chemiluminescent $NO_x$ analyzer (Thermo Environmental Instruments Inc., 42C, USA). Daily $NO_x$ analyzer calibrations were performed with $N_2$ (zero value) and NO and $NO_2$ gases certified by manufacturer analysis having a concentration of near 80% of the analyzer full-scale range (span value). During the adsorption experiment, analyses on column outlet concentrations of NO, $NO_2$, and $NO_x$ were controlled with software (Thermo Environmental Instruments Inc., C series, USA). Analytical data were captured every minute and read into a computer. To purge impurities from the system line before an adsorption was made it was flowed with He for 30 min at the flow rate of 500 mL/min at 473K. Then, the temperature was reset to experimental value, and the column was packed with adsorbent and re-purged with He for 10 min. Then, the zero value of $NO_x$ analyzer was checked before proceeding with the experiment.



### Surface Characterization

Before and after adsorption, surface analyses were conducted for samples by using SEM (Hitachi, S-1400, Japan) and static type ToF-SIMS (Perkin–Elmer, PHI-700 ToF-SIMS/SALI, USA).

The ToF-SIMS analysis was carried out using a system equipped with a two-stage reflectron-type analyzer. A low dose and pulsed $Cs^+$ primary ion beam, whose impact energy was 10 keV, was employed. The spectrometer was run at an operating pressure of $10^{-9}$ mbar. The primary ion beam was directed on a square area of 50 $\mu$m × 50 $\mu$m. The system was operated in high sensitivity mode with a pulse width of 50 nsec and with a beam current of 0.5 nA, resulting in a primary ion dose of approximately $4 \times 10^{11}$ ions per $cm^2$ analysis. The SIMS spectra were acquired over a mass range of $m/z = 1-100$ in negative modes.

## RESULTS AND DISCUSSION

### The Effect of KOH Impregnation

The conditions of experiment conducted to remove $NO_x$ from Run 1 to Run 7 are summarized in Table 1. In order to confirm the effect of K-IAC, the breakthrough curve of $NO_x$ comparing K-IAC (Run 2) and GAC (Run 1) in the absence of oxygen is shown in Fig. 2. The GAC became breakthrough as soon as the adsorption started and showed $C/C_0 = 0.75$ in 120 min. However, K-IAC was only about $C/C_0 = 0.25$. Comparing the adsorbed amounts, GAC recorded only 0.01 mmol $NO_x$/g GAC, whereas K-IAC showed 0.04 mmol $NO_x$/g K-IAC, which is four times higher



MARCEL DEKKER, INC.
270 Madison Avenue, New York, New York 10016

***Table 1.*** Conditions of Each Adsorption Experiment

| Run No. | Adsorbent | Adsorbate | NO Concentration (ppm) | $NO_2$ Concentration (ppm) | Contact Time (sec) | Linear Velocity (cm/sec) | Temperature (K) |
|---|---|---|---|---|---|---|---|
| 1 | GAC | $NO_2/N_2$ | 9 | 253 | 2.244 | 10.627 | 403 |
| 2 | K-IAC | $NO_2/N_2$ | 9 | 253 | 2.244 | 10.627 | 403 |
| 3 | K-IAC | $NO_2$/air | 3.6 | 138.2 | 0.185 | 10.803 | 303 |
| 4 | K-IAC | $NO_2$/air | 4.1 | 137.6 | 0.185 | 10.803 | 353 |
| 5 | K-IAC | $NO_2$/air | 3.8 | 147.6 | 0.185 | 10.805 | 403 |
| 6 | K-IAC | $NO_2/N_2$ | 3.6 | 144 | 0.185 | 10.807 | 403 |
| 7 | K-IAC | $NO_2$/air | 4.4 | 145.1 | 0.064 | 31.388 | 403 |



MARCEL DEKKER, INC.
270 Madison Avenue, New York, New York 10016

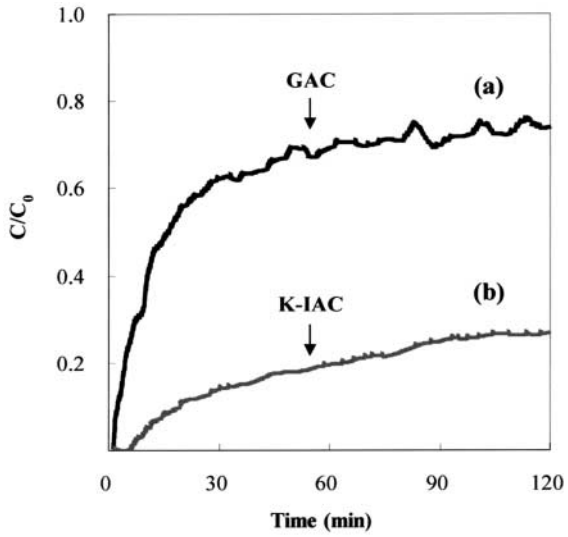


***Figure 2.*** A comparison of breakthrough curves over GAC and K-IAC: 262 ppm of $NO_x$ (with 253 ppm $NO_2$ and 9 ppm NO), flow rate = 591 mL/min ($N_2$ balance), sample amount = 12.725 g, adsorption temperature = 403K, linear velocity = 10.627 cm/sec, contact time = 2.244sec. (a) Run 1—$NO_x$/GAC; (b) Run 2—$NO_x$/K-IAC.

than that of GAC. Such a result confirms that K-IAC shows a good selectivity with $NO_x$, and it can be determined that KOH provided strong basic functional group to the GAC, playing an important role in providing adsorption site to allow selective adsorption of $NO_x$. That is, K-IAC at $NO_2$ adsorption is the effect of high selectivity of surface basic $OH^-$ ions with $NO_2$ due to KOH impregnation. This can be interpreted that the type of $NO_x$ adsorption on K-IAC forms oxide crystals of $KNO_x$ ($x = 2$ or 3) that are ionic chemical compounds due to potassium and occupies selective adsorption site. This is because potassium has a high reactivity and cannot exist as a single element substance but exists as a chemical compound bonded with other elements.

## Influence of Linear Velocity

Figure 3 shows a tendency of $NO_x$ adsorption for different linear velocities, i.e., 10.805 (Run 5) and 31.388 cm/sec (Run 7) after altering the flow rate at near 150 ppm $NO_x$/air. Comparing the adsorbed amount for 630 min, 10.805 cm/sec recorded only 0.35 mmol $NO_x$/g K-IAC, whereas 31.388 cm/sec of linear velocity showed 2.97 mmol $NO_x$/g K-IAC, which is 8.5 times higher than that of

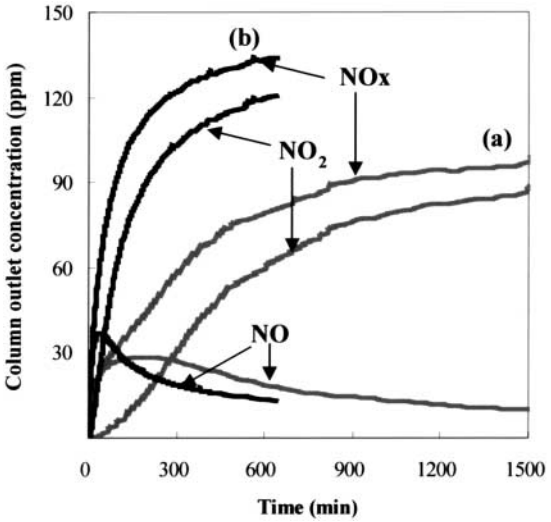


***Figure 3.*** $NO_x$ breakthrough curves over K-IAC for linear velocity variation: near 150 ppm of $NO_2$ (with 145–148 ppm $NO_2$ and 3.8–4.4 ppm NO), air balance (with 20.9% $O_2$), sample amount 1.067 g, adsorption temperature = 403K. (a) Run 5—10.805 cm/sec; (b) Run 7—31.388 cm/sec.

10.805 cm/sec. When the linear velocity is 31.388 cm/sec, gradients of concentration curves in the NO and the $NO_2$ became steeper. This is because even if the concentration of $NO_x$ is the same, the higher the linear velocity introduced in the column, the larger the absolute amount of $NO_x$ becomes, reducing the breakthrough time and reaching the saturated point faster. That is to say, as the linear velocity in K-IAC increases, the fast occurrence of catalytic conversion from $NO_2$ to NO leads to higher early concentration of NO and then the selective adsorption sites for $NO_x$ correlatively get lost in a quick mode. This increases the adsorbed amount for $NO_x$ at high linear velocity but results in relatively shorter breakthrough time.

## Influence of Temperature

Figure 4 shows the effect of temperature for $NO_x$ adsorption. It was performed at 303K (Run 3), 353K (Run 4), and 403K (Run 5) in the presence of oxygen. The experiment showed that breakthrough progressed slowly at a high temperature of 403K. Particularly, breakthrough was slower in the range between 353 and 403K than in the range between 303 and 353K. This phenomenon can be considered in three separate aspects. First, it is presumed to be because, as the

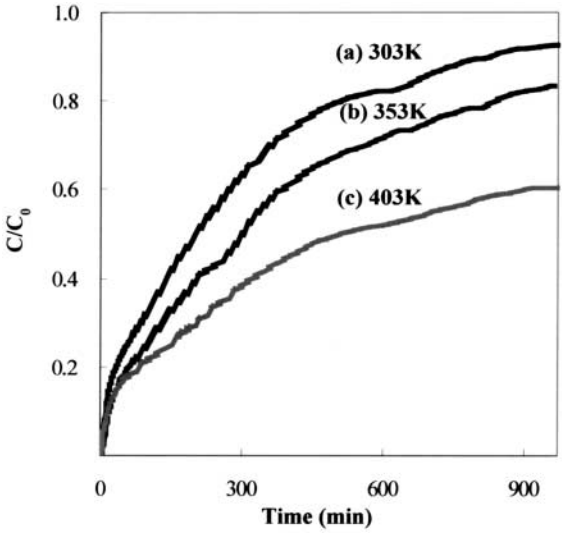


***Figure 4.*** $NO_x$ breakthrough curves over K-IAC for temperature variation: near 150 ppm of $NO_2$ (with 137–148 ppm $NO_2$ and 3.6–4.1 ppm NO), air balance (with 20.9% $O_2$), sample amount 1.067 g, linear velocity = 10.803–10.805 cm/sec, contact time = 0.185 sec. (a) Run 3—303K; (b) Run 4—353K; (c) Run 5—403K.

temperature increases, $NO_2$ that reacts with KOH goes beyond activation barrier, and its collision fraction, which has a large collision energy enough to cause reaction with $K^+$, increases. Secondly, it is because, as in Eq. (1),

$$O_2 \rightarrow O_{ads} \tag{1}$$

chemisorption of oxygen in an atomic state to K-IAC is achieved better at high temperature. As $NO_2$ adsorption is in progress, there also occurs a conversion phenomenon of NO to $NO_2$ by the chemisorbed oxygen. Thus, it can be said that adsorptivity improved compared with nonexistence of oxygen. Thirdly, in the condition of low temperature at which $H_2O$ can exist on the surface, it may lose adsorptivity by blocking the pore by being condensed on the surface as $HNO_3$ with $NO_2$ adsorption.

## Influence of Oxygen

Researchers have already reported the fact that adsorption efficiency increases considerably by the addition of oxygen in $NO_x$ adsorption (13,23). Figure 5 shows a breakthrough curve for $NO_x$ in the states where oxygen exists or does not. As a result,

as shown in Fig. 5 (a, Run 6), when no oxygen was present, the adsorbed amount of $NO_x$ was 1.40 mmol $NO_x$/g K-IAC from 960 min of reaction, while in the presence of oxygen as shown in Fig. 5 (b, Run 5), the adsorbed amount is 0.55 mmol $NO_x$/g K-IAC. The oxygen addition showed a 2.5 times higher adsorbed amount for $NO_x$. It seems that the difference is caused by Eq. (2).

$$NO + O_{ads} \rightarrow NO_{2\,ads} \tag{2}$$

Therefore, Fig. 5 (b) can be interpreted as adsorption efficiency improved in a repeated process in which NO generates due to $NO_2$ adsorption and, with the addition of oxygen, reaction of Eq. (2) occurs again according to Eq. (1) through atomic-state oxygen, which was chemisorbed to the surface at different adsorption sites.

## Surface Characterization

### Scanning Electron Microscopy Study

Figure 6 shows the images observed, by using SEM at the magnification of 300×, 1000×, and 30,000× from top to bottom, about the process in

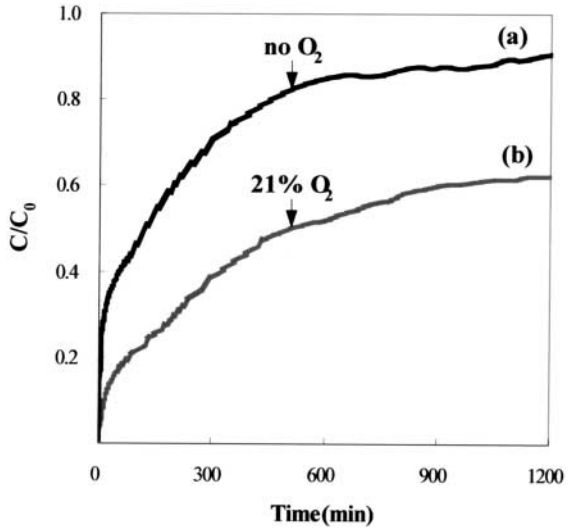


***Figure 5.*** $NO_x$ breakthrough curves the absence and the presence of oxygen: near 150 ppm of $NO_2$ (with 144–148 ppm $NO_2$ and 3.6–3.8 ppm NO), sample amount = 1.067 g, adsorption temperature = 403K, linear velocity = 10.805–10.807 cm/sec, contact time = 0.185 sec. (a) Run 6—no $O_2$; (b) Run 5—21% $O_2$.





MARCEL DEKKER, INC.
270 Madison Avenue, New York, New York 10016

which NO and $NO_2$ are adsorbed to K-IAC. It shows that the surface of nonadsorbed K-IAC in Fig. 6(a) was clear and countless pores exist in various sizes. In terms of types of pores, it has a structure of branched pores in which mesopores exist in macropores and micropores develop in mesopores. These pores show a phenomenon in which they gradually get filled as certain crystals from micropores to macropores in the order (a) → (c) → (d) of Fig. 6. In addition, it can be expected that the selective adsorption sites get lost with the growth of some generated crystals that block the pores. At less than 373K, $HNO_3$ ($T_b \approx 393$K) can be generated on the surface during the reaction due to $H_2O$ production (13). The condition of this experiment is 403K and, therefore, it is expected that the pores are occupied by $KNO_x$, which constitute the stable-crystal state by forming ionic bond with $NO_x$ by $K^+$. Figure 6(b) shows the SEM image performed for NO. NO is adsorbed into micropores in a small quantity in the form of $NO_2$ by oxygen complex type functional group that exists in the existing GAC, which is different from Fig. 6(a).

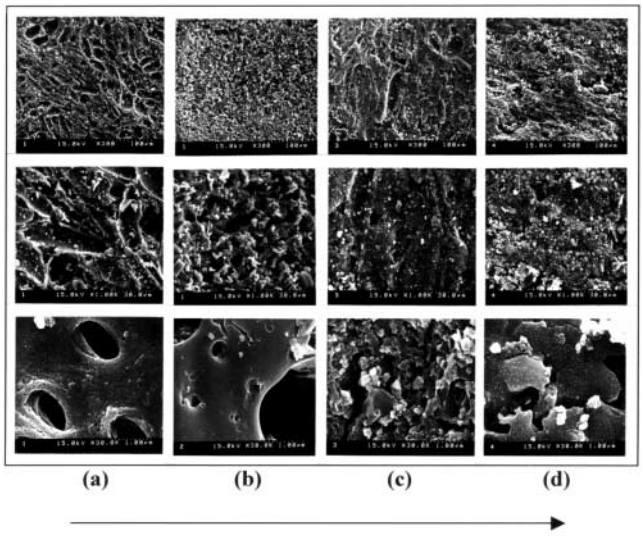


***Figure 6.*** The SEM photograph of K-IAC: (a) nonadsorbed; (b) 2 hr $NO/N_2$ adsorbed ($C/C_0 = 0.98$); (c) 2 hr $NO_2/N_2$ adsorbed ($C/C_0 = 0.48$); (d) 50 hr $NO_2/N_2$ adsorbed ($C/C_0 = 0.97$).





MARCEL DEKKER, INC.
270 Madison Avenue, New York, New York 10016

Time of Flight Secondary Ion Mass Spectrometry Study

The surface composition and chemistry of K-IAC were studied using ToF-SIMS. In dealing with gas–solid reaction, researchers generally use x-ray photoelectron spectroscopy (XPS) and Auger electron spectroscopy (AES) that have a good quantification, provide information on chemical states, and allow easy data interpretation. In these instruments, however, the elemental sensitivity limit is 0.1% and molecular identification is impossible. To analyze low concentration $NO_x$ in which adsorption occurs on K-IAC that is composed of organic and inorganic complex including hydrogen, it can be quite informative to use ToF-SIMS that has a very good sensitivity even at the ppm unit and in which simultaneous analysis of organic and inorganic compound is possible (24,25). While ToF-SIMS has the above-mentioned merits, it has the following shortcoming as an instrument. In quantitative analysis, the ToF-SIMS is not proportionate to the surface concentration absolutely and fragment peaks make interpretation difficult. Therefore, it is necessary to do careful calibration.

In this experiment, background was calibrated by comparing Inductively coupled plasma-atomic emission spectroscopy (ICP-AES; Labtest Plasmascan 710, USA) and ToF-SIMS for a sample whose concentration was known. At the time of analyzing $NO_x$ adsorbed K-IAC, their tendencies were interpreted by comparison with nonadsorbed K-IAC, increasing the reliability of the data.

In Fig. 7, the results of surface analysis are indicated by using ToF-SIMS with sample under the conditions of nonadsorbed and $NO_x$ adsorbed K-IAC of $C/C_0 = 0.42$. In the results from polarity of ions detected from analysis, the negative range that provides information on main peaks in the interaction between KOH and $NO_x$ was 1–100 *m/z*. In $NO_x$ adsorbed K-IAC, the following main ions were discovered. In the negative spectrum, the peaks of increased ions compared with nonadsorbed K-IAC were $CN^-$ ($m/z = 26$), $CNO^-$ ($m/z = 42$), $NO_2^-$ ($m/z = 46$), and $NO_3^-$ ($m/z = 62$), while the peaks of decreased ions were $H^-$ ($m/z = 1$), $C^-$ ($m/z = 12$), $CH^-$ ($m/z = 13$), $O^-$ ($m/z = 16$), $C_2^-$ ($m/z = 24$), $C_2H^-$ ($m/z = 25$), $O_2^-$ ($m/z = 32$), $KO^-$ ($m/z = 55$), and $CO_3^-$ ($m/z = 60$). When the nonadsorbed and $NO_x$ adsorbed K-IAC are compared, $NO_2^-$ and $NO_3^-$ that hardly existed before adsorption were generated after adsorption at high intensity. Therefore, we could understand that $NO_x$ adsorption progressed at selective adsorption sites in the form of $NO_2^-$ and $NO_3^-$. That is to say, $NO_2^-$ and $NO_3^-$ after adsorption analysis by ToF-SIMS bonded on the surface with $K^+$ and produced crystals of $KNO_2$ and $KNO_3$. Some reduction of $OH^-$ after adsorption indicates that there still remain selective adsorption sites for $NO_x$. $OH^-$ that participated in selective adsorption produces $H_2O$ through reaction with $NO_x$. At this time, it vaporizes at the experimental condition of 403K and does not exist on the surface. However, $OH^-$ that forms a bonding as nonreactive KOH and occupies a selective adsorption site appears with SIMS analysis due to high $T_b$. In





MARCEL DEKKER, INC.
270 Madison Avenue, New York, New York 10016

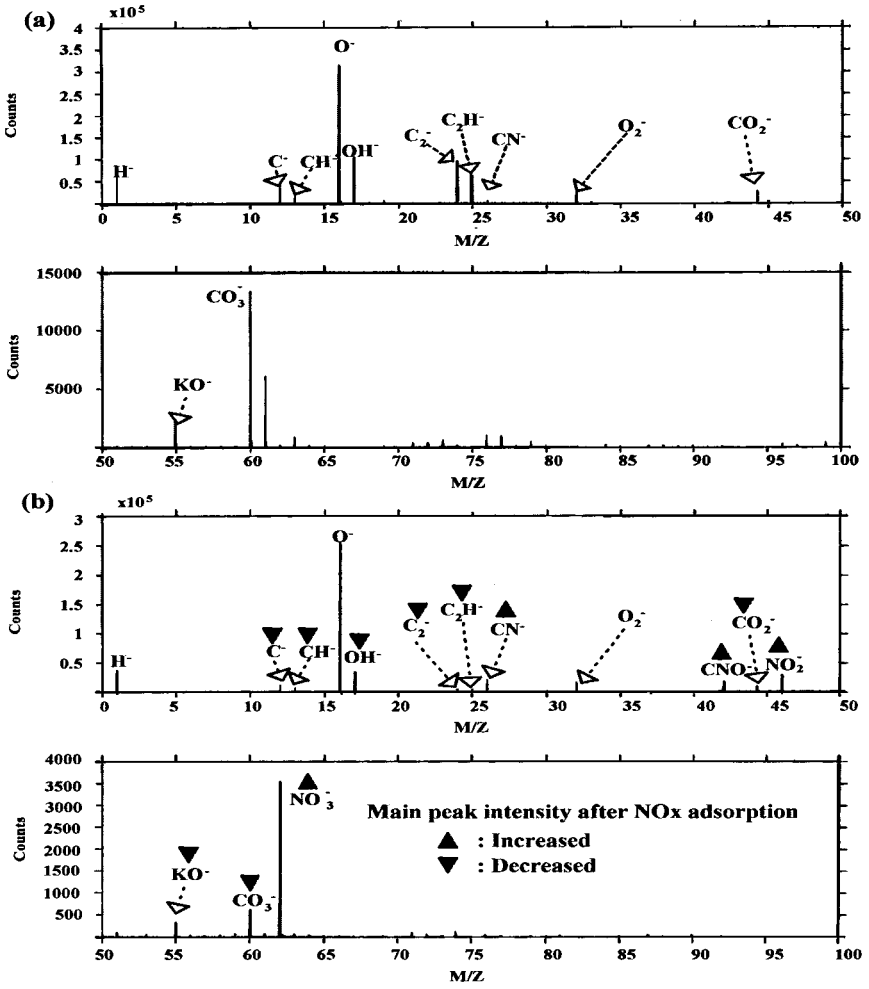


***Figure 7.*** The ToF-SIMS negative spectra: (a) nonadsorbed on K-IAC; (b) $NO_x$ adsorbed on K-IAC ($C/C_0 = 0.48$, adsorbed for 2 hr with near 150 ppm of inlet $NO_x$ concentration at 403K, Run 6).

the ToF-SIMS spectra of K-IAC, the $C_xH^-$ ($x = 1, 2$) and $C_x^-$ ($x = 1, 2$) peaks were assigned to aromatic carbons with and without bonds to hydrogen, respectively (26). The $CO_2^-$ and $CO_3^-$ peaks were due to oxygen complex functional group of activated carbon. As in Fig. 7, ion counts of nitrogen-containing species are increased on the K-IAC by $NO_x$ adsorption. It can be considered that $CN^-$ is converted with bond cleavage of $C_xH^-$, $CO_2^-$, and $CO_3^-$





MARCEL DEKKER, INC.
270 Madison Avenue, New York, New York 10016

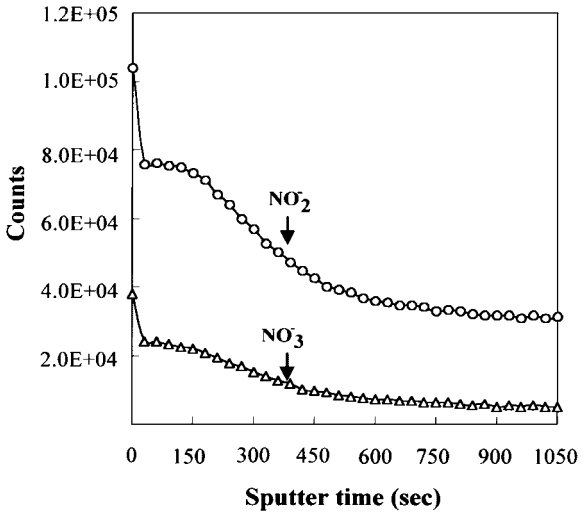


***Figure 8.*** The SIMS depth profile of K-IAC for $NO_3^-$ and $NO_2^-$ ions obtained from K-IAC with $C/C_0 = 0.48$ (adsorbed for 2 hr with near 150 ppm of inlet $NO_x$ concentration at 403K, Run 6).

by $NO_x$ adsorption. Reduction of $C_x^-$, $C_xH^-$, $CO_2^-$, and $CO_3^-$, and formation of $CNO^-$ support this fact.

## Secondary Ion Mass Spectrometry Depth Profiles

In SIMS depth analysis, secondary ion counts were indicated as a function of sputtering. Sputter depth is about 60 Å for every 1 min on the basis of Si. $NO_2^-$, $NO_3^-$, and $KO^-$ among the main negative peaks analyzed in Fig. 7 showed a sputter-depth profile. It illustrates differences in the number of count by sputter time of main ionic species for nonadsorbed K-IAC and $NO_x$ adsorbed K-IAC that shows a breakthrough progress of $C/C_0 = 0.42$.

Figure 8 shows the depth profiles of $NO_2^-$ and $NO_3^-$ with diffusion of $NO_x$ into pores. Due to a bond formation with the potassium ion, $NO_x$ exist in pores as $KNO_2$ and $KNO_3$. In depth profile results, ion counts of $NO_2^-$ and $NO_3^-$ decreased rapidly to about 42,557 and 9647, respectively, due to predominant external diffusion on the surface by $NO_x$ up to 450 sec and slowly decreased and stayed at about 31,207 and 5069 up to 1050 sec. The differences in the relative counts ratios of $NO_2^-$ to that of $NO_3^-$ are about three times for up to 450 sec and six times for up to 1050 sec. That is to say, in accord with the increase in the sputter time





MARCEL DEKKER, INC.
270 Madison Avenue, New York, New York 10016

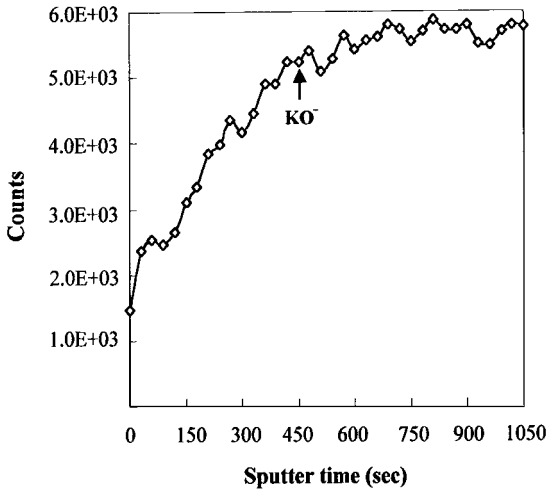


***Figure 9.*** The SIMS depth profile of K-IAC for $KO^-$ ion obtained from K-IAC with $C/C_0 = 0.48$ (adsorbed for 2 hr with near 150 ppm of inlet $NO_x$ concentration at 403K, Run 6).

(or depth), ion counts of $NO_3^-$ decrease extremely. This phenomenon is due to predominant $KNO_3$ on the external surface of K-IAC. In addition, the existence of $KNO_3$ is dependent on the oxidation of produced $KNO_2$ on the K-IAC by $NO_x$ adsorption.

Figure 9 shows the depth profiles for $KO^-$. In the depth profile for $KO^-$, the question of whether KOH is connected directly with the existence of selective adsorption sites or not was verified. The sputter time increased rapidly from 0 to 450 sec. After 450 sec, it showed a tendency to increase slowly. The pattern of this phenomenon was contrary to that of depth profile at $NO_2^-$ and $NO_3^-$ in Fig. 8. When examined by depth profile, $NO_2^-$ and $NO_3^-$ were adsorbed more at the selective adsorption sites up to a sputter time of 450 sec when there occurred a relatively higher $NO_x$ adsorption. From this, we can conclude that increased $NO_2^-$ and $NO_3^-$ brought a decreased phenomenon of $KO^-$ as in Fig. 9. That is, KOH provides selective adsorption sites for $NO_x$.

## Predicted Chemical Reaction by a Breakthrough Trend and Surface Characterization

$NO_x$ had the following characteristics in the chemical reaction with KOH, which was impregnated to the surface. Fig. 10 shows a representative





MARCEL DEKKER, INC.
270 Madison Avenue, New York, New York 10016

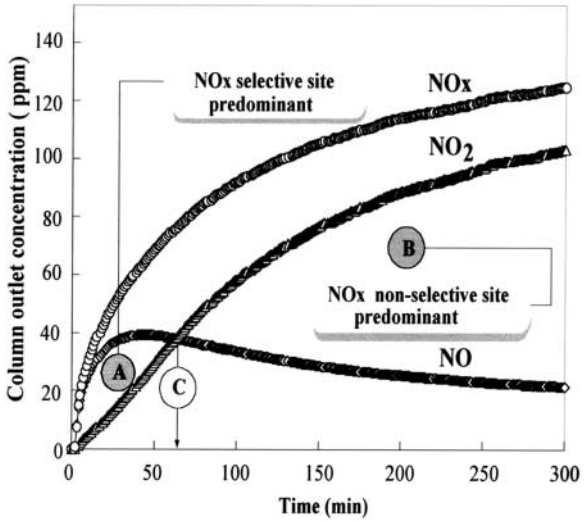


***Figure 10.*** Representative concentration curve of $NO_x$ adsorption on K-IAC.

tendency on K-IAC of $NO_2$ adsorption in the experiment. $NO_x$ selective adsorption sites were predominant in the surface state of A area compared with that of B area, so more NO was generated than $NO_2$ in A area. The B area becomes the opposite of A area. The B area is the point at which concentration of $NO_2$ becomes higher than that of NO. Even afterwards, however, NO was generated continuously for a long time. Here, it can be argued that, to improve adsorption capacity of $NO_x$, the condition of experiment in which A area is made broad by delaying C point is an optimum condition of this reaction.

Figure 11 shows the expected reaction mechanism from adsorption of $NO_x$ on K-IAC. $NO_2$ is adsorbed to the surface by chemical reaction with KOH and generates $H_2O$ by forming $KNO_2$ and $KNO_3$ that are composed of stable ionic bond-type crystals. With continuous adsorption with $NO_2$, the generated $KNO_2$ is oxidized in the end, becomes $KNO_3$ and releases NO. At low temperature, however, $H_2O$ forms $HNO_2$ and $HNO_3$ with $NO_2$ adsorption. $HNO_2$ exists as a thermodynamic equilibrium state with $NO_x$, and $HNO_3$ may become a factor that reduces adsorptivity by blocking the selective adsorption sites.

It can be said that the effect of impregnation of KOH is to provide basic $OH^-$ ions to GAC and play a role that delays the rate of oxidation to $KNO_3$ by $NO_x$. In addition, $K^+$ helped the stable adsorption of $NO_x$ on K-IAC.

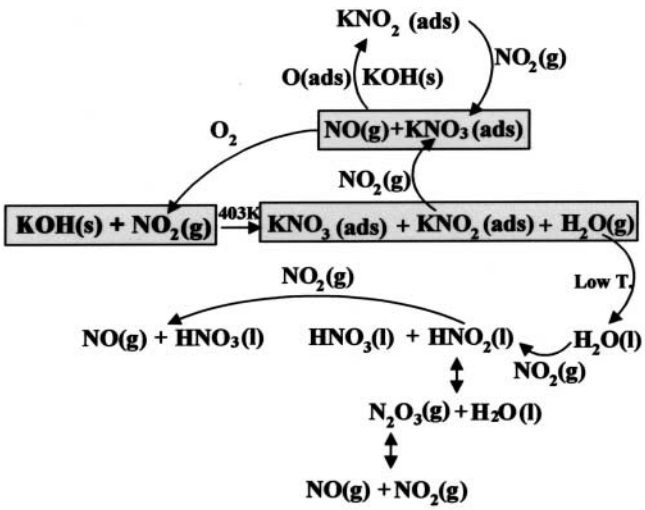


***Figure 11.*** Predicted reaction mechanism of $NO_x$ over K-IAC.

## CONCLUSION

This study was done, first, to understand the adsorption characteristics of $NO_x$ through a breakthrough experiment by using a fixed-bed adsorption column and secondly, based on this, to examine the surface chemistry according to $NO_x$ that was adsorbed on the K-IAC. The K-IAC confirmed that the adsorption was mostly due to chemical reaction. $NO_2$ adsorption had an adsorptivity that was four times higher than that of GAC. $NO_2$ is adsorbed by reaction with impregnated KOH, and then NO is generated because of it. At 403K, which is an established experimental condition, good adsorptivity is expected because the existence of $H_2O$ and $HNO_3$, which may be generated in the surface due to side reaction, may be blocked and chemisorption of oxygen is relatively well done. When oxygen is present, this NO was adsorbed as $NO_2$ by oxygen that was chemisorbed in the atomic state on KIAC and increased the adsorptivity. The main chemical composition was analyzed for pre- and post-adsorption of $NO_x$ by using ToF-SIMS and surface chemistry and was confirmed by performing SIMS depth profile. Decrease of $C_x^-$, $C_xH^-$, $CO_2^-$, and $CO_3^-$ on K-IAC with progress of $NO_x$ adsorption has to do with the increased conversion to $CN^-$ and creation of $CNO^-$ supports it. The $OH^-$ in existing K-IAC generated $H_2O$ by reaction with $NO_x$, vaporized, and decreased at 403K, which was the experimental condition.

That the selective adsorption site was composed of KOH can be explained as a phenomenon in which $NO_2^-$ and $NO_3^-$ produce crystals of $KNO_2$ and $KNO_3$

by $K^+$ and increase the surface distribution. A depth profile of $KO^-$ confirmed that KOH provides a selective adsorption site for $NO_x$. The studies on adsorption reaction and surface chemistry showed that the basic surface $OH^-$ ions, which were well developed on the surface due to impregnation of KOH to K-IAC, showed high selectivity with $NO_2$ and improved adsorptivity by leading basic character on K-IAC and delaying the rate of oxidation to $KNO_3$. In addition, $K^+$ by $NO_2$ adsorption played a catalyst role that adsorbs crystals of $KNO_2$ and $KNO_3$ that are ionic compounds to the surface.

## NOMENCLATURE

| | |
|---|---|
| $C$ | effluent gas concentration (ppm) |
| $C_0$ | influent gas concentration (ppm) |
| $T_b$ | boiling temperature (K) |

## ACKNOWLEDGMENTS

We are grateful to Dr. Yeon-Hee Lee of the Korea Institute of Science and Technology for her valuable discussion and experimental help with ToF-SIMS and SIMS depth profiles.

## REFERENCES

1. Pereira, C.J. Environmentally Friendly Processes. Chem. Eng. Sci. **1999**, *54*, 1959–1973.
2. Radojevic, M. Reduction of Nitrogen Oxides in Flue Gases. Environ. Pollut. **1998**, *102* (S1), 685–689.
3. Neathery, J.K.; Rubel, A.M.; Stencel, J.M. Uptake of $NO_x$ by Activated Carbons; Bench-Scale and Pilot-Plant Testing. Carbon **1997**, *35* (9), 1321–1327.
4. Yun, J.H.; Choi, D.K.; Kim, S.H. Adsorption Equilibria of Chlorinated Organic Solvents onto Activated Carbon. Ind. Eng. Chem. Res. **1998**, *37* (4), 1422–1427.
5. Yun, J.H.; Choi, D.K.; Kim, S.H. Equilibria and Dynamics for Mixed Vapors of BTX in an Activated Carbon Bed. Am. Inst. Chem. Eng. J. **1999**, *45* (4), 751–760.
6. Köpsel, F.W.; Halang, S. Catalytic Influence of Ash Elements on $NO_x$ Formation in Char Combustion Under Fluidized Bed Conditions. Fuel **1997**, *76*, 345–351.

7. Harding, A.W.; Brown, S.D.; Thomas, K.M. Release of NO from the Combustion of Coal Chars. Combust. Flame **1996**, *107*, 336–350.
8. Nandhakumar, I.S.; Li, Z.Y.; Palmer, R.E.; Amos, R. LEED and Resonance EELS Study of the $(NO)_2$ Dimer on Graphite. Surf. Sci. **1995**, *329*, 184–192.
9. Zhu, Z.; Liu, Z.; Liu, S.; Niu, H. Adsorption and Reduction of NO over Activated Coke at Low Temperature. Fuel **2000**, *79*, 651–658.
10. Aho, M.J.; Pirkonen, P.M. Effect of Pressure, Gas Temperature and $CO_2$ and $O_2$ Partial Pressures on the Conversion of Coal-Nitrogen to NO, $N_2O$ and $NO_2$. Fuel **1995**, *74*, 1677–1681.
11. Mochida, I.; Kawabuchi, Y.; Kawano, S.; Matsumura, Y.; Yoshikawa, M. High Catalytic Activity of Pitch-Based Activated Carbon Fibres of Moderate Surface Area for Oxidation of NO to $NO_2$ at Room Temperature. Fuel **1997**, *76*, 543–548.
12. Huang, H.Y.; Yang, R.T. Catalyzed Carbon–NO Reaction Studied by Scanning Tunneling Microscopy and Ab Initio Molecular Orbital Calculation. J. Catal. **1999**, *185*, 286–296.
13. Kong, Y.; Cha, C.Y. $NO_x$ Adsorption on Char in Presence of Oxygen and Moisture. Carbon **1996**, *34*, 1027–1033.
14. Kalberer, M.; Ammann, M.; Gäggeler, H.W.; Baltensperger, U. Adsorption of $NO_2$ on Carbon Aerosol Particles in the Low ppb Range. Atmos. Environ. **1999**, *33*, 2815–2822.
15. Mochida, I.; Kawabuchi, Y.; Kawano, S.; Matsumure, Y.; Yoshikawa, M. High Catalytic Activity of Pitch-Based Activated Carbon Fibres of Moderate Surface Area for Oxidation of NO to $NO_2$ at Room Temperature. Fuel **1997**, *76*, 543–548.
16. Illán-Goméz, M.J.; Linares-Solano, A.; Salinas-Martínez de Lecea, C. NO Reduction by Activated Carbon. 6. Catalysis by Transition Metals. Energy Fuels **1995**, *9*, 976–983.
17. Illán-Goméz, M.J.; Brnadán, S.; Linares-Solano, A.; Salinas-Martínez de Lecea, C. $NO_x$ Reduction by Carbon Supporting Potassium-Bimetallic Catalysts. Appl. Catal. B **2000**, *25*, 11–18.
18. Zhu, Z.H.; Lu, G.O. Catalytic Conversion of $N_2O$ to $N_2$ over Potassium Catalyst Supported on Activated Carbon. J. Catal. **1999**, *187*, 262–274.
19. García-García, A.; Illán-Gomez, M.J.; Linares-Solano, A.; Radovic, L.; Salinas-Martienez, C. Potassium-Containing Briquetted Coal for the Reduction of NO. Fuel **1997**, *76*, 499–505.
20. Lott, S.E.; Gardner, T.J.; McLaughlin, L.I.; Oelfke, J.B.; Matlock, C.A. Nitrogen Oxide Adsorbing Material. US Patent 5,795,553, August 18, 1998.
21. Boehm, H.P. Acidic and Basic Properties of Hydroxylated Metal Oxide Surfaces. Discuss. Faraday Soc. **1972**, *52*, 264–275.






MARCEL DEKKER, INC.
270 Madison Avenue, New York, New York 10016

22. Spevack, P.; Deslandes, Y. ToF-SIMS Analysis of Adsorbate/Membrane Interactions. Appl. Surf. Sci. **1996**, *99*, 41–50.
23. Aurora, M.R.; John, M.S. The Effect of Low-Concentration $SO_2$ on the Adsorption of NO from Gas Over Activated Carbon. Fuel **1997**, *76*, 521–526.
24. Vickers, P.E.; Castle, J.E.; Watts, J.F. Quantification Routines for Adsorption Studies in Static Secondary Ion Mass Spectrometry and the Effect of Ionisation Probability. Appl. Surf. Sci. **1999**, *150*, 244–254.
25. Lamontagne, B.; Semond, F.; Adnot, A.; Roy, D. SIMS Investigation of the Si(111) Oxidation Promoted by Potassium Overlayers. Appl. Surf. Sci. **1995**, *90*, 447–454.
26. Roy, C.; Darmstadt, H.; Benallal, B.; Amen-Chen, C. Characterization of Naphtha and Carbon Black Obtained by Vacuum Pyrolysis of Polyioprene Rubber. Fuel Process. Technol. **1997**, *50*, 87–103.

Received November 2000
Revised May 2001

# Request Permission or Order Reprints Instantly!